Springer

KSME

Journal of Mechanical Science and Technology 28 (8) (2014) 3311~3323
www.springerlink.com/content/1738-494x
DOI 10.1007/s12206-014-0742-x

Model-based optimization of injection strategies for SI engine gas injectors †

Stefano Beccari, Emiliano Pipitone*, Marco Cammalleri and Giuseppe Genchi

Department of Chemical, Management, Computer and Mechanical Engineering, University of Palermo, Viale delle Scienze, Palermo, Italy

(Manuscript Received July 15, 2013; Revised April 1, 2014; Accepted April 17, 2014)

Abstract

A mathematical model for the prediction of the mass injected by a gaseous fuel solenoid injector for spark ignition (SI) engines has been realized and validated through experimental data by the authors in a recent work [1]. The gas injector has been studied with particular reference to the complex needle motion during the opening and closing phases. Such motion may significantly affect the amount of injected fuel. When the injector nozzle is fully open, the mass flow depends only on the upstream fluid pressure and temperature. This phenomenon creates a linear relationship between the injected fuel mass and the injection time (i.e. the duration of the injection pulse), thus enabling efficient control of the injected fuel mass by simply acting on the injection time. However, a part of the injector flow chart characterized by strong nonlinearities has been experimentally observed by the authors [1]. Such nonlinearities may seriously compromise the air-fuel mixture quality control and thus increase both fuel consumption and pollutant emissions (SI engine catalytic conversion systems have very low efficiency for non-stoichiometric mixtures). These nonlinearities arise by the injector outflow area variation caused by needle impacts and bounces during the transient phenomena, which occur in the opening and closing phases of the injector. In this work, the mathematical model previously developed by the authors has been employed to study and optimize two appropriate injection strategies to linearize the injector flow chart to the greatest extent. The first strategy relies on injection pulse interruption and has been originally developed by the authors, whereas the second strategy is known in the automotive engine industry as the peak and hold injection. Both injection strategies have been optimized through minimum injection energy considerations and have been compared in terms of linearization effectiveness. Efficient linearization of the injector flow chart has been achieved with both injection strategies, and a similar increase in injector operating range has been observed. The main advantage of the pulse interruption strategy lies on its ease of implementation on existing injection systems because it only requires a simple engine electronic control unit software update. Meanwhile, the peak and hold strategy reveals a substantial lack of robustness and requires expressly designed injectors and electronic components to perform the necessary voltage commutation.

Keywords: Gas injector; Injection strategy; Spark ignition engine

1. Introduction

Experimental observation by the authors in a previous work [1] revealed the existence of strong nonlinearities in the lower part of a typical spark ignition (SI) engine gas injector flow chart (i.e., the diagram that reports the injected mass as a function of injection time). These nonlinearities can cause unstable control of engine air-fuel ratio and may thus compromise both engine efficiency and pollutant emissions. The literature research conducted by the authors showed the existence of numerous studies on the simulation and modeling of internal combustion engine injection systems. Compression ignition (CI) engines are usually equipped with high-pressure (1600 bar-2000 bar) common rail injectors [2, 3], which can be activated by either a solenoid or a piezoelectric element. These injectors use the high pressure of fuel to move the needle and open the nozzle [4].

SI engines may be port injected or direct injected. The former usually employ low-pressure (3 bar-10 bar, depending on fuel type) injectors [2, 3, 5], whereas the latter may require higher injection pressure (100 bar-500 bar) [3, 6].

Although considerable research on injection system simulation is available in the literature, only a few works cover the dynamic modeling of injector needle motion. Such motion significantly influences the injector diagram and is the focus of this paper. In relation to common rail injection systems, needle motion has been well discussed in the literature. For example, the fluid-dynamic model presented in a previous work [7] predicts the injection pressure variations to derive proper injection control laws. The model developed in Ref. [8] also predicts the needle lift and injection rate for different injection pressures. The common rail piezoelectric injector model realized in Ref. [9] considers both the hydraulic part (fluid flow, discharge coefficients) and the mechanical part

*Corresponding author. Tel.: +39 091 23897280, Fax.: +39 091 23860840
E-mail address: emiliano.pipitone@unipa.it
† Recommended by Associate Editor

(needle movement, seats elastic deformation) to predict different flow rate profiles. As regards gasoline direct injection, the model developed in Ref. [10] refers to a piezoelectric injector and compares the capability of lumped parameters and distributed parameters to describe needle motion and piezoelectric element behavior. The dumping effect of liquid fuels completely suppresses needle bounces. However, none of the above works [7-10] reports any injector flow chart nonlinearities. The experience of the authors confirms the absence of nonlinearities in the injector flow chart when using gasoline. Thus, this problem is unique to gas injection systems.

The modeling of gas injection in an SI engine was introduced in Ref. [11], which explored the details of fuel spray formation and mixture with air. The dynamic behavior of the injector needle is discussed in Ref. [12], in which different model predictive control schemes were presented for the control of an electromagnetically actuated mass-spring-damper system for automotive applications. The natural gas injection system modeled in Ref. [13] presents control strategies for the optimization of injection system operation with a focus on the fluid-dynamic behavior of the whole injection system (fuel rail, pressure control valve, and injectors). However, despite focusing on gas injections, none of these works [11-13] deal with the nonlinearities produced by needle bounces during the opening and closing phases of the injector. Only the work presented in Ref. [14] deals with the complex needle motion during opening and closing phases with a focus on the suppression of needle bounces to prevent fatigue stress damage. Unlike the approach followed in the present paper, however, the implementation of the method proposed in Ref. [14] requires substantial modification of the injector power supply system.

The presence of a nonlinear zone in the injector flow chart, particularly its correlation with the needle motion, has not yet been studied in detail. This consideration motivated the authors to develop a mathematical dynamic model of the gas injector and to study a proper injection strategy with the aim of linearizing the injector flow chart. This strategy will improve the air-fuel mixture quality control and thus minimize both fuel consumption and pollutant emissions.

2. Solenoid injector dynamics

A typical gaseous fuel, such as liquefied petroleum gas (LPG) and compressed natural gas (CNG), multi-point injection system of modern SI engine is composed of the following main elements (Fig. 1): a gas tank (6), a pressure regulator and filter (2 and 3), and a fuel rail (7), which feeds each injector (4). In the setup shown in Fig. 1, fuel is injected into the inlet duct (port injection). The regulator reduces the gas pressure from the high level in the tank (where LPG is stored at approximately 10 bar and CNG at approximately 200 bar) to the low level in the fuel rail (approximately 2 bar for LPG and 10 bar for CNG). The regulator is usually warmed by the engine coolant to avoid freezing because of gas expansion. The regulator is sometimes connected to the intake manifold to maintain a constant pressure difference between the fuel rail and the air manifold. The flow through the gas injector can be assumed as equivalent to the flow through the convergent nozzle. In chocked flow condition (i.e. supposing that the usual ratio between fuel rail pressure and manifold pressure is ≥ 2), the gas flow depends only on pressure and temperature upstream the injector. This phenomenon makes the injected mass directly proportional to the injector opening duration. The electronic control unit (ECU) adjusts the injected fuel mass and thus acts on the injection time (i.e., the duration of the injection pulse), the values of which are functions of engine speed and load. These values are stored in memory by means of appropriate tables. A more precise control of air-fuel ratio is achieved by means of closed-loop control with the use of the lambda sensor output signal.

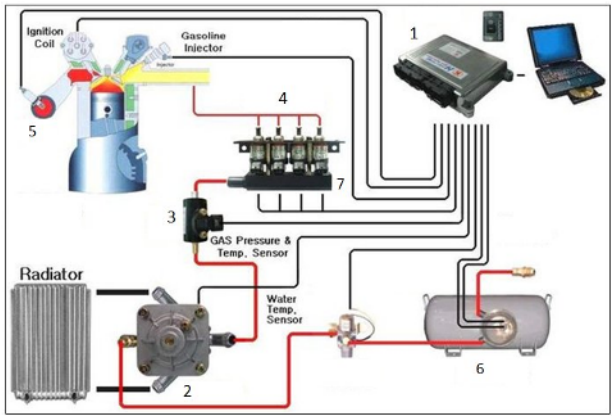

Fig. 1. Gaseous fuel multi point injection setup (1 ECU, 2 pressure regulator, 3 filter valve, 4 gas injectors, 5 lambda sensor, 6 gas tank, 7 fuel rail).

Fig. 2(a) shows a cutaway of the solenoid fuel injector used in the test [3] and Fig. 2(b) the typical electrical circuit used to energize the injector solenoid. This circuit is composed of a power supply, an injector solenoid, and a power transistor, which is usually activated by the transistor-to-transistor logic (TTL) pulses generated by the engine ECU. The injector is mainly composed of a mechanical part, which is the needle, and an electric part, which is a solenoid. These two parts interact and influence each other through the electromagnetic field. The needle movement influences the solenoid current, which consequently acts on the needle through the electromagnetic force.

When the solenoid is not energized (i.e., the electrical circuit is open) the needle is kept in a closing position by both the fuel pressure and the spring load. When the ECU activates the transistor, which can be considered as a digital switch, the electrical circuit closes (Fig. 2(b)) and the current rises in the solenoid windings according to the R-L circuit law. The needle is then thrust by the electromagnetic force and moves from the closed toward the open position, thus knocking against the stop surface at the end of the lift. The needle bounces and moves toward the closed position, where another impact may occur. Under the action of the electromagnetic field, the nee-

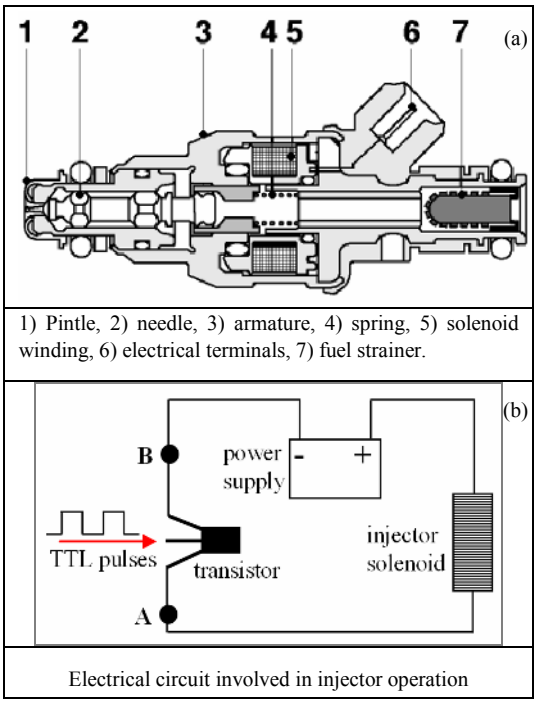

Fig. 2. Cutaway of fuel injector used in test (a); and scheme of injection electrical circuit (b).

dle will be pushed toward the open position, thus producing other bounces. If the injection time is sufficiently long, the needle will conclude all bounces and will remain in open position when thrust by the electromagnetic field. Once the injection time is finished, the ECU deactivates the transistor, which opens the circuit to produce an instantaneous drop in the solenoid current. The needle is then forced by the fuel pressure and the spring load to return to the closed position, thus knocking against the closed position seat and producing other bounces. Figs. 3 and 4 show the output signal from an accelerometer mounted on the armature of an injector used for test during the injector opening and closing phases. The strong impacts that occur both in the opening and closing phases cause prominent spikes on the accelerometer output signal.

The diagrams also show the measured solenoid current, which is characterized by the presence of several cusps during the opening phase. Given the reciprocal interaction between needle movements and coil-winding current [1, 14], the abrupt velocity variation during an impact causes a rapid change in the current first derivative. These current cusps are absent in the closing transient because after the end of the injection, the electric circuit is open, and the solenoid current is null.

Fig. 3 also shows that for the tested injector fed with air at 10 bar, the bounces of the opening phase continue for approximately 4 ms. Meanwhile, in the closing phase (see Fig. 4), the duration is shorter at approximately 3 ms. The importance of these bounces relies on the variations that they produce on the injected mass because the instantaneous flow section depends on the needle position. Therefore, assuming a

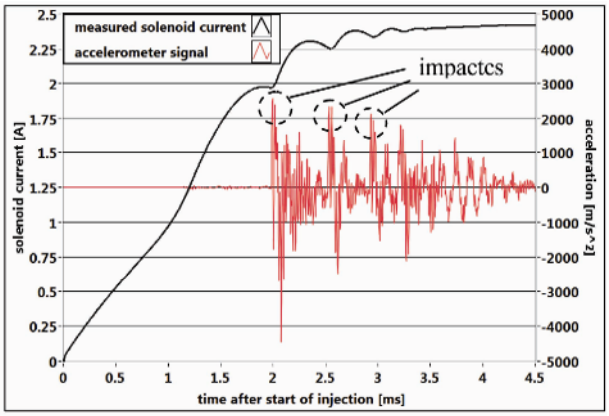

Fig. 3. Solenoid current and armature accelerations during injector opening phase.

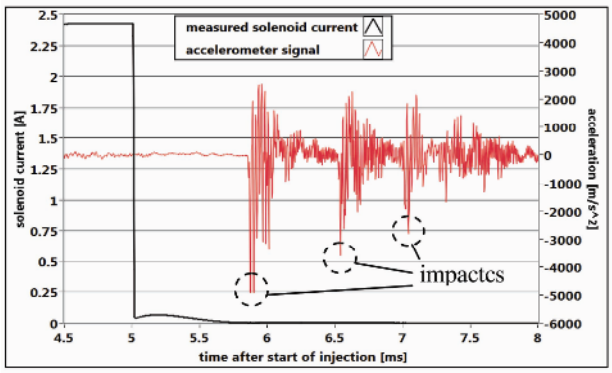

Fig. 4. Solenoid current and armature accelerations during injector closing phase.

linear correlation between flow section area and needle position, the injected mass depends on the integral of the needle position. This phenomenon implies that for injection times lower than the opening phase duration (≈4 ms for the injector tested fed with air at 10 bar), the injected mass exhibits nonlinear dependence on time because the outflow section is subjected to continuous variations. Moreover, given that the impact energy of the needle on the opening stop surface depends on its kinetic energy, which in turn is related to the duration of the electromagnetic force applied and hence to the injection time, the needle movement itself depends on the duration of the injection. Such dependence introduces a further cause of variation of the injected mass. The final result is the clear nonlinear relation between injected mass and injection time shown in the injector flow chart in Fig. 5. This diagram shows the measured injected mass for each of the injection times imposed to the injector fed with air at 10 bar. It is worth to remark that this diagram does not represent the integral of the gas mass flow as function of time, but rather the measured total injected mass at the end of each single injection, the duration of which is the injection time Δt. As can be noted the needle bounces significantly affect the total injected mass for injection durations shorter than the bounces duration (≈ 4 ms).

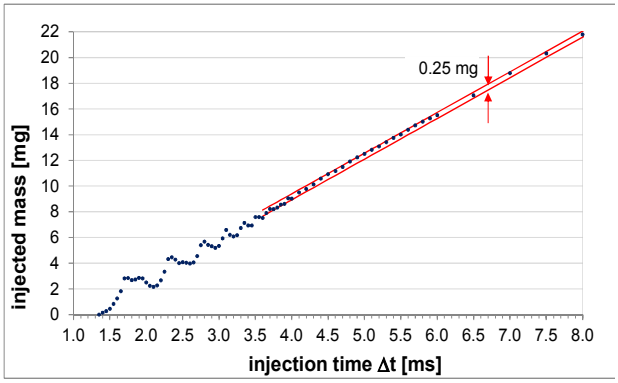

Fig. 5. Experimental injector flow chart obtained with air at 10 bar.

The experimental data used in this study have been collected by feeding a Bosch EV1 natural gas injector with air at 8, 9, and 10 bar absolute pressure with the use of a 13 V DC power supply. The injector has been actuated by using 0 V to 5 V TTL pulses generated by a National Instruments counter board PCI-6602 programmed with LabVIEW. A transistor was used to transform the low power digital pulses into the high current square waveforms necessary for injector solenoid excitation (Fig. 2). A Bruel & Kjaer Cubic DeltaTron 4502 accelerometer was placed on the injector armature to detect the needle impacts. A clamp-on ammeter LEM PR20 with 20 kHz frequency response was used to acquire the solenoid current, whereas the air mass flow was measured by means of a Bronkhorst mini CORI-FLOW M13, a Coriolis-type mass flow meter with a measuring range of 0.1 ÷ 2.0 kg/h and an accuracy of ± 0.2% of the measured value. The injector was activated with frequencies ranging from 10 Hz to 70 Hz to obtain mass flows within the measurable range. For each injection time, the experimental injected mass m_{exp} was derived from the measured mass flow $\dot{m}$ and injection frequency f_{inj}

$$m_{\text{exp}} = \frac{\dot{m}}{f_{inj}}. \tag{1}$$

All the necessary quantities have been acquired by means of a National Instruments DAQ board PCI-6133, employing a sample frequency of 400 kHz and using the generated TTL pulse as trigger for data acquisition. For each injection time, the complete waveforms of input voltage, solenoid current, and accelerometer output were recorded for 100 consecutive injections, whereas mass flow, gas pressure, and temperature were recorded as mean values over 100 injections. In this way, for each injection pressure tested, a complete injector chart (with an example shown in Fig. 5) reporting the total injected gas mass for each injection time between 1 and 8 ms can be obtained.

The non-monotonic behavior of the flow chart arises from the flow section variations caused by the needle bounces [1], the intensities of which are related to the needle kinetic energy. Such energy depends on the duration of the applied electromagnetic force. During the opening phase, the needle frequently reverses its motion because of the bounces on the two stop surfaces, whereas the electromagnetic force always acts in the same direction. This phenomenon implies that depending on the needle velocity, the electromagnetic thrust may accelerate or slow down the needle and thus change its effect in terms of needle kinetic energy and consequently in terms of the integral of needle position, which is proportional to the injected mass. Therefore, increasing the injection time during the opening phase may have opposite effects on the injected mass, depending on the needle position and velocity. This conclusion has been confirmed by experimental observation of the solenoid current and armature acceleration waveforms, together with mass flow data acquisition conducted for air injection duration between 1.8 and 2.5 ms. Such observation was accomplished through a 100 MHz oscilloscope.

When the injection time is sufficiently long to enable the needle complete all the opening bounces (i.e., ≥ 4 ms for 10 bar air pressure), all the opening and closing transient phenomena identically repeat at each single injection and thus have no effect on the total injected mass, which then becomes a linear function of the injection time. As shown in Fig. 5, the deviation from the linear trend remains in the range ±0.25 mg for injection times higher than 4 ms.

The nonlinearities of the injector flow chart can cause inaccurate control over the engine air-fuel ratio, which can consequently result in both higher fuel consumption and higher pollutant emissions because of the catalytic converter lower efficiency caused by the non-stoichiometric air-fuel mixture. These nonlinearities have not been observed using gasoline. Thus, this study focuses on gaseous fuels injector dynamics.

Moreover, in recent experimental works [15, 16], the simultaneous combustion of a gaseous fuel (CNG or LPG) and gasoline in a SI engine was tested to achieve significant improvement both in engine efficiency and pollutant emissions with respect to pure gasoline operation mode, which requires rich mixtures at full load. The addition of CNG (or LPG) to gasoline-air mixtures strongly improves knocking resistance [17], thus enabling the engine to run at full load with a global stoichiometric mixture and with optimal combustion phase (i.e. spark advance). This third operating mode of bi-fuel engines, called Double Fuel combustion, requires small amounts of gaseous fuel, thus forcing the injectors to work in the non-monotonic zone of the injector flow chart, where the control on air-fuel ratio is poor.

3. Mathematical model

In a previous work Ref. [1], the authors realized a mathematical model for the simulation of the complex needle motion during the opening and closing phases of the injector to predict the amount of fuel injected for each injection time. The model has been calibrated by means of the experimental data obtained on the test bench with the use of a natural gas injector fed with air at 9 bar. This model was successfully validated

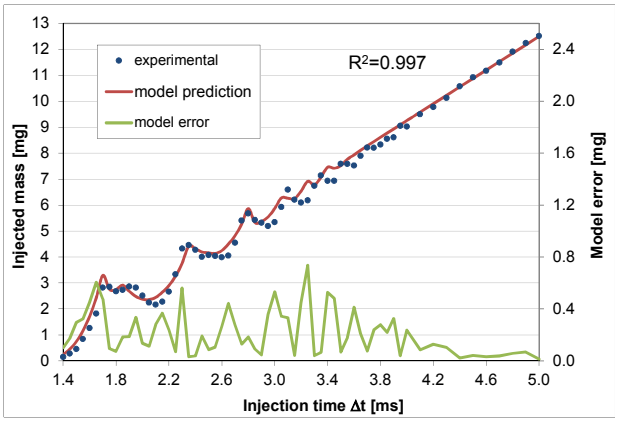

Fig. 6. Comparison between measured and computed injected mass (air pressure 10 bar).

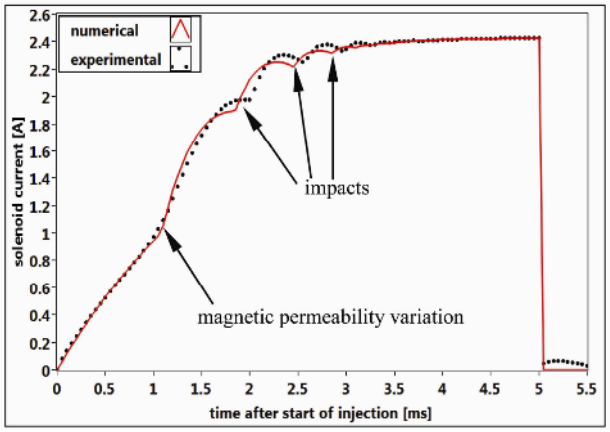

Fig. 7. Model output: solenoid current and needle displacement as function of time (injection time Δt = 5 ms).

by the experimental data obtained by injecting air at 8 and 10 bar. The results shown in this paper refer to the injection of air at 10 bar absolute pressure. Fig. 6 shows the comparison between measured and simulated injector flow charts. A very good fit was found between experimental data and model prediction because the nonlinearities of the experimental diagram are accurately replicated by the model. Fig. 6 also shows the error (i.e. difference between calculated and measured injected mass) distribution with mean and maximum values of 0.22 and 0.74 mg, respectively. In all the cases, the model evaluation accuracy was comparable with the test measurement uncertainties [1], which are unrelated to mass flow measurement errors (always less than 1%) but rather depends on the injected mass oscillation around the mean values.

The predictive capacity of the model was further confirmed by the comparison between the measured and the evaluated solenoid current under the same conditions of air pressure and injection time.

Fig. 7 shows the good agreement between the experimental and numerical current during the injector opening phase; the first cusp is attributed to the variation of the steel magnetic permeability, whereas the other cusps are associated with the

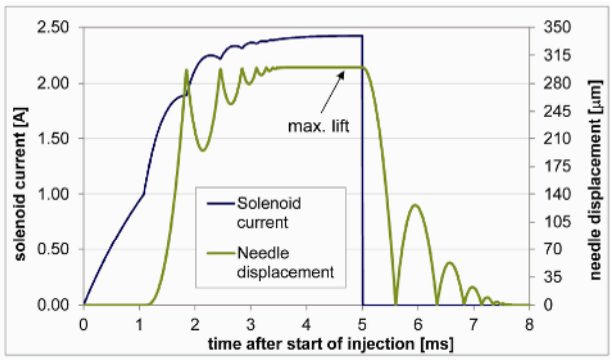

Fig. 8. Measured and simulated solenoid current as function of time.

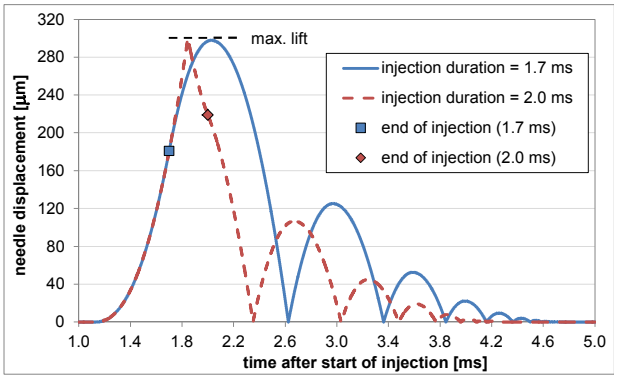

Fig. 9. Simulated needle displacement for two injections with Δt = 1.7 and 2.0 ms.

sudden speed change of the needle because of the impacts on the seat surface.

Fig. 8 shows the typical model output, that is, the solenoid current and the needle displacement as a function of time. In particular, the diagram refers to a 5 ms injection of air at 10 bar. Notably, the opening phase bounces are evident both in the needle displacement and in the solenoid current. These bounces have a duration of approximately 3.6 ms. As a consequence, this duration is also the minimum injection time of the linear part in the simulated flow chart shown in Fig. 6.

The closing phase bounces have a duration of approximately 2.5 ms and are only evident in the displacement waveform, because the transistor (Fig. 2(b)) is deactivated at the end of the injection. This deactivation opens the electric circuit ad causes the current to drop to zero immediately.

Fig. 9 shows the needle displacement evaluated by the model for two different injection durations, that is, 1.7 and 2.0 ms, with air at 10 bar. In the case of the 2.0 ms injection, the electromagnetic force still acts after the first impact, which slows down the needle. The successive impacts of the needle have lower energy, thus resulting in smaller bounces. The results show that the 2.0 ms injection is characterized by a lower integral of the needle position, which means a lower integral of the mass flow and, thus a lower injected mass. The

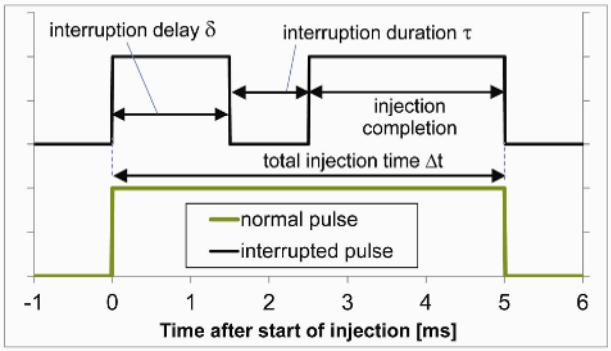

Fig. 10. Injection pulse with and without interruption.

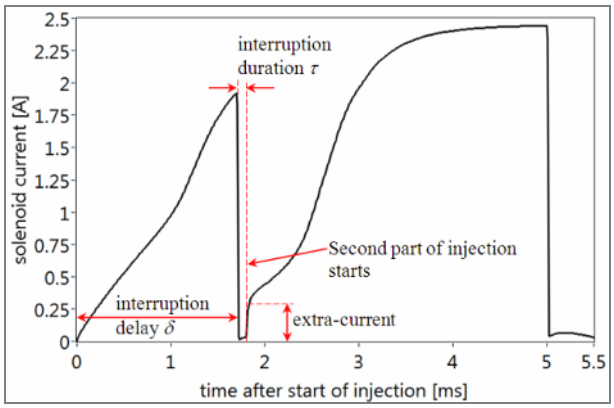

Fig. 11. Measured solenoid current for an interrupted injection pulse (injection time = 5 ms).

simulated injector flow chart in Fig. 6 confirms that with air at 10 bar, a 1.7 ms injection causes a higher injected mass than a 2.0 ms injection.

4. Pulse interruption strategy

The needle bounces on the stop surfaces originate from the excess kinetic energy acquired by the needle during the opening lift, which in turn is attributed to the excess energy transferred through the electromagnetic field and thus by the solenoid. Therefore, the needle should arrive at the opening stop surface with no kinetic energy and be maintained in this position by the electromagnetic thrust to avoid any bounce. This condition can be achieved by the proper modulation of the solenoid current to reduce the electromagnetic thrust on the needle progressively during the lift. This process involves the minimum energy necessary to shift the needle from the closed to the open position. The whole excess of energy transferred to the needle, with respect to the minimum required, is completely dissipated during bounces by the mechanical friction between the needle and guides, by the gas viscous forces, and by the energy loss at each impact. Grater movement and impact of the needle causes more energy to be dissipated.

However, the modulation of the solenoid current requires the modulation of the voltage supplied to the injector solenoid, which is constant and equal to the battery voltage, as is usually the case in automotive engines. Given the difficulty in supplying variable voltage to the solenoid, the energy transferred to the needle during the opening lift can be modulated elsewhere by acting on the duration of the injection pulse. This pulse can be divided into two: the first part dedicated to shifting the needle from the closed to open position without bounces, and the second part dedicated to maintaining the needle in the open position and letting the fuel flow. The authors hence focused on this division, which can be realized by the simple interruption of the injection pulse, characterized by two parameters: the interruption delay δ with respect to the start of injection, and the duration τ, both pointed out in Fig. 10.

The authors used the mathematical model previously developed to determine the values of the two parameters that prevent needle bounces and that linearize as much as possible the injector characteristic flow chart.

Before starting the research on the optimal interruption parameters, the model was further improved, so that it can adequately consider a phenomenon concealed by the first experimental campaign. As reported in Fig. 11, the solenoid current measured during an interrupted injection shows a kind of extra current that substantially modifies the current waveform and hence the needle motion. This additional current is due to the partial discharge of the energy accumulated by the solenoid, which occurs during the injection interruption. Details on this phenomenon and on the model modifications introduced by the authors are given further in Appendix A.

Once refined, the model is employed to perform several simulations to determine the optimal values that are to be assigned to the interruption parameters δ and τ to avoid any needle bounce. According to the explanation above, this condition should also minimize the energy E employed in the needle shift from the closed to open position. The authors thus adopted as objective function ϕ of the search algorithm the energy transferred to the needle in the opening phase:

$$\varphi = E = \int_0^{\Delta t^*} V \cdot i \cdot dt \tag{2}$$

where Δt^* is the time interval necessary for the needle to complete all the opening phase bounces and stop in the open position, V the solenoid supply voltage, and i the solenoid current.

As a first step, the authors considered the injection time of 5 ms, which, as reported in Fig. 8, results in several bounces in the opening phase transient. A simple search algorithm was employed because an entire matrix of interruption delay δ (ranging from 1.55 ms to 1.76 ms with steps of 0.003 ms) and duration τ (ranging from 0.01 ms to 0.15 ms with steps of 0.002 ms) was tested to evaluate the objective function ϕ on the base of the resulting simulation output. This procedure enabled the tracing of the ϕ surface shown in Fig. 12 as a function of the two variables, the delay δ and duration τ. The

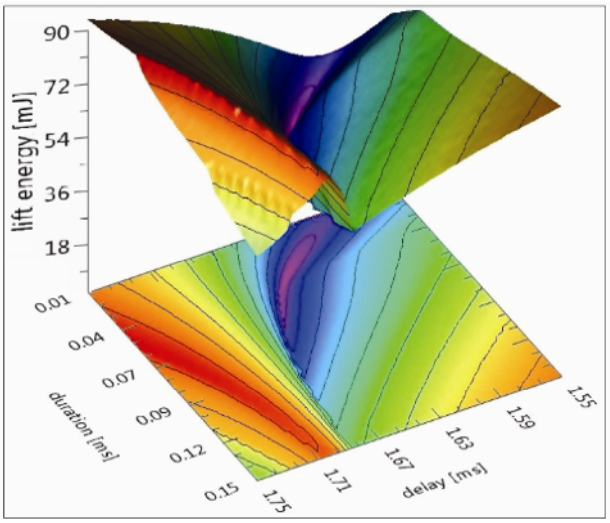

Fig. 12. Surface of the opening phase energy (mJ) and its contour plot as function of the two interruption parameters.

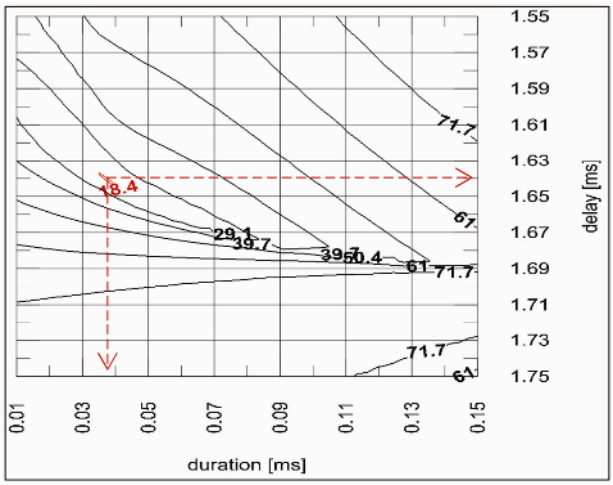

Fig. 13. Contour plot of the opening phase energy (mJ) as a function of the two interruption parameters.

figure shows a visible absolute minimum region, whose coordinates represent the best (minimum energy) values of the interruption delay and duration. Fig. 13 also shows a contour plot of the ϕ surface, the best interruption parameters of which are $\delta = 1.64$ ms and $\tau = 0.038$ ms.

As a result, the optimal injection pulse interruption of the injector tested and fed with air at 10 bar has a very short duration and should therefore be placed before the first impact occurs. The effects of these optimal interruption parameters on the 5 ms injection of air at 10 bar are reported in Fig. 14 in terms of both the solenoid current and needle displacement. The modulation of the injection energy actuated through the pulse interruption has the effect of allowing the needle to reach the open stop surface without impacts and hence without producing bounces. The best result is obtained by preventing the first impact from occurring. Once the needle is at rest

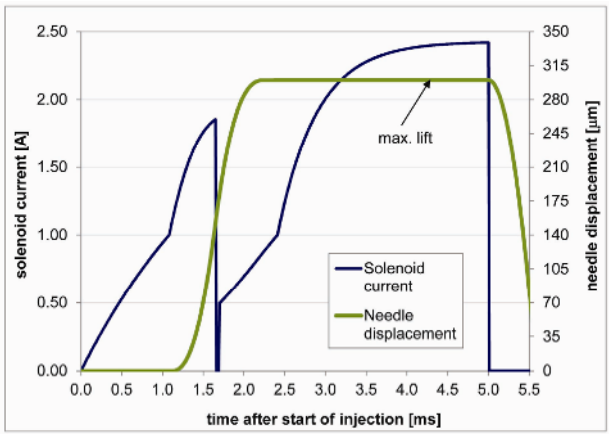

Fig. 14. Solenoid current and needle displacement predicted by the model employing the optimal interruption parameters.

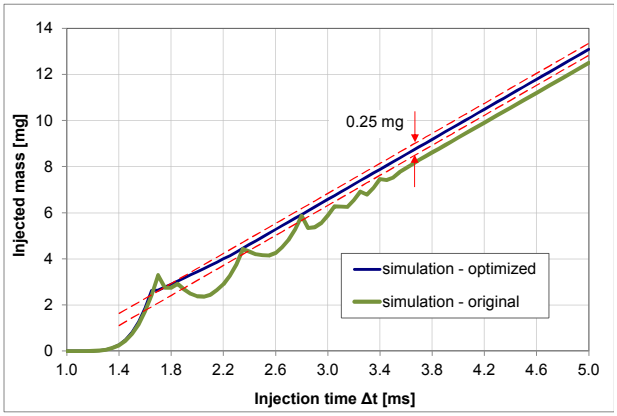

Fig. 15. Comparison of the simulated original and optimized injector flow charts.

in the open position, the mass flow remains constant and the injected mass becomes a linear function of the injection time.

Fig. 15 shows the injector flow chart obtained by adopting the same interruption parameters for each injection. The figure shows that a satisfying linearization is obtained, because most of the nonlinearities are now suppressed, and the injector characteristic is now a monotone function of the injection time. Its linearity lies in the range of ±0.25 mg for an injection time of as low as 1.75 ms, which corresponds to an injected mass of 2.8 mg. The linear behavior of the injector is now extended well below the 4 ms and 9 mg of the original (simulated) flow chart of Fig. 6. For comparison, the flow chart without pulse interruption is also shown in Fig. 15.

The time interval between the first rising front and the last falling front of the injection pulse is conventionally considered the injection time, as shown in Fig. 10.

According to these results, a very good linearization of the injector flow chart can be obtained through a simple injection pulse modulation. This kind of power supply strategy can easily be implemented in the current production engines through a simple ECU programming, without any hardware

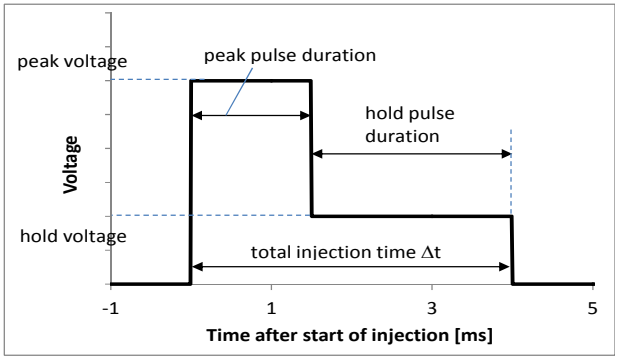

Fig. 16. "Peak and hold" injection pulses.

change. The suppression of gas injectors needle bounces has also been studied [14] to prevent fatigue stress damages: the method proposed in that study, however, relies on a substantial modification of the injector power supply system.

5. Peak and hold injection strategy

The second injection strategy examined in this work is known in the automotive industry as the "peak and hold" injection. This approach relies on feeding the solenoid injector with two consecutive different current levels: the first (the peak current) is high enough to shift the needle quickly from a closed to an open position, whereas the second (the hold current) is sufficient to hold the needle in open position during fuel flow. Originally developed to shorten as much as possible the overall injection time, this second injection strategy has been taken into consideration since it also allows a modulation of the energy transferred to the needle, thereby acting on the solenoid current (and hence on the power supply voltage), rather than on the pulse duration. However, the low voltage of the hold phase requires the use of low-impedance injectors, whereas the rapid commutation between the two different voltage levels requires complex and expensive electronic components. Thus, contrary to the pulse interruption modulation, this strategy cannot be implemented without hardware modifications and additional cost.

A comparison with the pulse interruption strategy was conducted on equal terms, minimum energy optimization was also performed for the "peak and hold" strategy, which was used in the mathematical model to activate the transistor with two successive injection pulses, the peak and the hold. These impulses correspond to two different voltage levels and are employed to obtain both the peak and the hold current (see Fig. 16).

The latter is considered the minimum current needed to hold the needle in open position, thereby counterbalancing the closing forces that result from the gas pressure and the spring. For this reason, this hold current strictly depends on the gas pressure and implies a voltage of 5.78 V for the injector fed with air at 10 bar. The hold pulse duration can be determined once the peak pulse duration is known, because both are complementary and sum up the total injection time, as shown in Fig. 16.

Table 1. "Peak and hold" injections characteristics.

Point of Fig. 18	Peak voltage [V]	Peak duration [ms]	Start of needle movement [ms]
A	24	0.56	0.54
B	13	1.13	1.13
C	35	0.38	0.36

The voltage V_p and duration Δt_p of the peak pulse are interdependent, because a high peak pulse voltage results in a strong opening thrust on the needle and hence requires less time to move the needle. By contrast, a low peak voltage requires a more time to shift the needle from closed to the open position and therefore a long peak phase duration.

Given a certain peak voltage (which is significantly higher than the hold voltage), the peak pulse duration should be fixed for the same purpose as that of the previous injection strategy (i.e. to shift the needle from closed to open position without causing impact and bounces). This process is accomplished following the same principle of the minimum energy required. Hence, for each couple of peak pulse parameters (i.e. peak voltage and duration), the total energy transferred to the needle during the opening phase is evaluated by means of Eq. (2). A second surface is obtained, as shown together with its contour plot in Fig. 17. The latter is repeated and clearly observable in Fig. 18. The minimum energy required in the opening phase with the "peak and hold" injection is as expected almost the same as that required by the pulse interruption strategy (i.e. about 18 mJ for the injection of air at 10 bar) (see also Fig. 13).

Table 1 also shows that, for each peak voltage considered, the resulting optimal peak duration is almost equal to the time required to make the needle leave the closing stop surface. This equivalence means that the optimal peak voltage is necessary as long as the needle remains in closed position. Once the needle leaves the closing seat surface, it requires only the hold current to move toward the open stop surface without bounces. A higher voltage during this movement increases the kinetic energy, thereby causing an impact on the closing surface. This phenomenon explains the presence of a sudden rising front just next to the minimum energy region in Fig. 17. Once the optimal peak voltage is fixed, a slight decrease in the peak duration causes the needle to remain closed, and the injection does not occur. This fault condition is represented for mathematical continuity purposes by a constant conventional high value of the energy required. The presence of this rising front however reveals the very low robustness of the optimal "peak and hold" injection, whose practicability therefore requires precisely determining and executing the peak phase voltage and duration.

Fig. 19 shows the needle displacement obtained from the simulation using the "peak and hold" parameters of points A, B, and C of Fig. 18 (all simulation refers to the injection of air at 10 bar). As expected, no bounces are evident, which confirms the optimization performed through the minimum en-

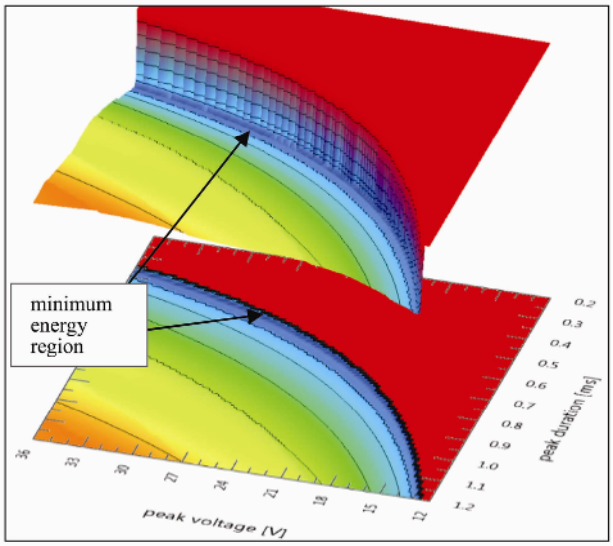

Fig. 17. Surface of the opening phase energy [mJ] and its contour plot as a function of the two peak pulse parameters.

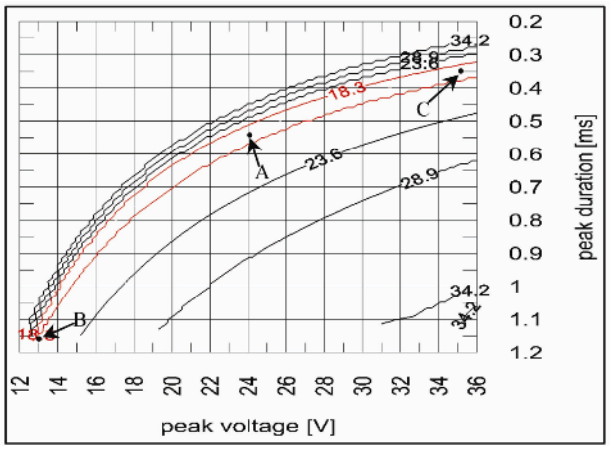

Fig. 18. Contour map of the opening phase energy [mJ] as a function of the two peak pulse parameters.

ergy concept. The needle displacement obtained from the optimal pulse interruption strategy is also shown for comparison. Fig. 20 shows that the latter is characterized by a high velocity in the opening phase, because of the high current involved during the needle movement. The three current waveforms related to the "peak and hold" injections reveal a cusp, which is caused by the commutation from the peak to the hold supply voltage. As observed above, this commutation occurs once the needle starts to move.

The injector flow charts obtained from the "peak and hold" injections are reported in Fig. 21. A good linearization has been achieved, because the nonlinearities of the original injector flow chart are almost completely removed.

The flow chart obtained through the pulse interruption strategy is also shown for comparison. It lies between the 24 and the 13 V "peak and hold," and its trend is as good as that of the "peak and hold" injections, starting from a injection time

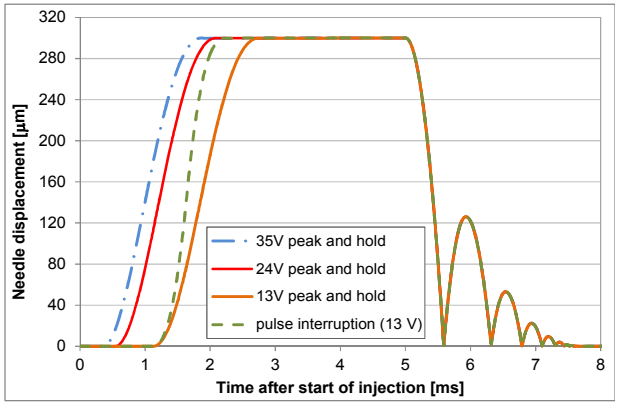

Fig. 19. Comparison between the needle displacement in the "peak and hold" injection and that in the pulse interruption strategy.

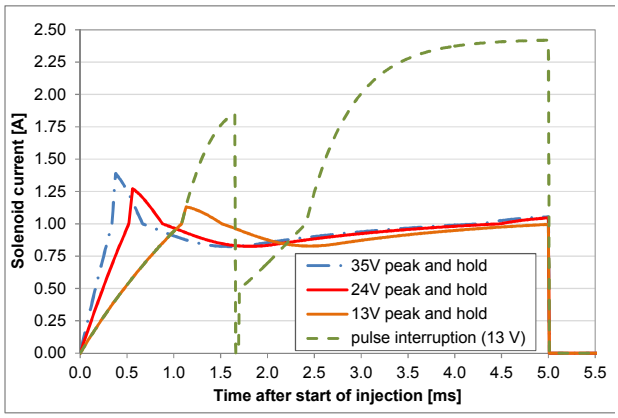

Fig. 20. Comparison between the solenoid current of the "peak and hold" injection and that of the pulse interruption strategy.

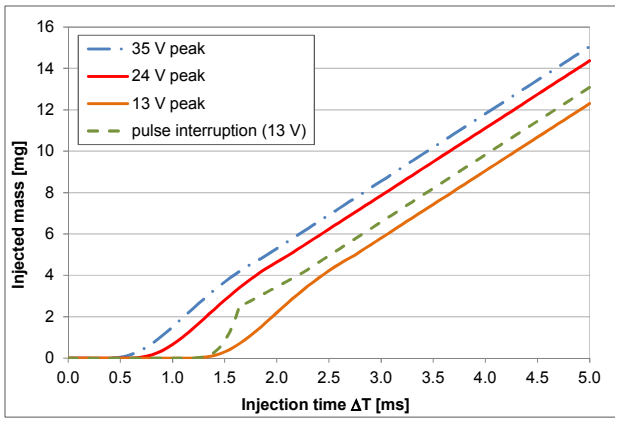

Fig. 21. Comparison of the linearized injector flow charts.

of 1.65 ms. The three peak voltages used yield almost the same good results in terms of injector flow chart linearization. However, increasing the peak voltage advances the needle opening phase, thus facilitating the increase of the injected mass for the same total injection time. As a result, passing from 13 V to 35 V peak voltage causes an injected mass increase of about 3 mg. This injected mass increase can be use-

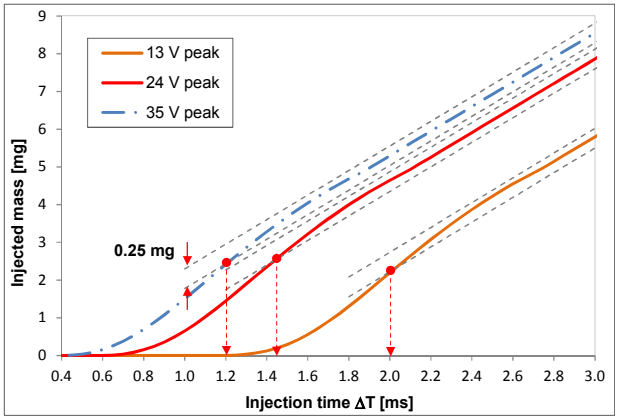

Fig. 22. Comparison of the "peak and hold" injector flow charts.

ful when high amounts of fuel are required (e.g. for engine supercharging purpose), and when the total time available for injection is limited.

Fig. 22 shows a portion of the "peak and hold" flow charts limited to an injection time below 3 ms. The flow chart in the 13 V "peak and hold" injection enters a linearity range of ±0.25 mg at an injection time of 2.0 ms, which corresponds to an injected mass of 1.74 mg. This result is similar to that obtained from the pulse interruption strategy. The flow chart in the 24 V peak voltage enters the linearity range at an injection time of 1.45 ms, which corresponds to an injected mass of 2.58 mg. Increasing the peak voltage to 35 V further improves the flow chart, which lies within a linearity range of ±0.25 mg at an injection time of 1.20 ms and injected mass of 2.42 mg.

Given that the reliable injector operating range is limited within the linear zone of the flow chart, both "peak and hold" and "pulse interruption" strategies increase this range and reduce both the minimum injection time and the minimum injectable mass with respect to the conventional operating mode.

The pulse interruption strategy can easily be implemented in the current injection systems by simply reprogramming the engine ECU. By contrast, implementing the "peak and hold" strategy is expensive, because it requires expressly designed electronic components to manage the voltage commutation.

6. Conclusions

In a previous work [1] the authors realized a mathematical model for the simulation of the complex needle motion of a natural gas injector needle, and for the evaluation of the injected mass. Once calibrated by means of experimental data collected on the test bench using a natural gas injector, the model was proven to be capable of predicting with unexpected accuracy the amount of gas injected at each injection time and of reproducing faithfully the nonlinearities of the real injector flow chart, which originate from the needle impacts and bounces that characterize the opening and closing phase of the injector.

In the present paper, the authors employed the model to study and compare possible injection strategies to linearize as much as possible the gas injector flow chart. The analysis of the needle motion, together with some fundamental considerations of energy conservation, led to the definition of a proper objective function, which guided the authors toward one possible solution to the problem. The main advantage of this solution is that it can easily be implemented in the current engine ECU without any hardware modification or additional costs. The implementation consists of the proper modulation of the energy transferred to the needle through injection pulse interruption to avoid impacts and bounces.

A second injection strategy known in the automotive industry as the "peak and hold" injection was also examined for its capability to modulate the energy transferred to the needle acting on the solenoid current rather than on the pulse duration. As in the case of the "pulse interruption" strategy, this strategy was optimized using the same minimum energy concept.

Once implemented in the model, both injection strategies proved to be effective in the linearization of the injector characteristic and in widening the injector operating range. The implementation of the "peak and hold" strategy however requires expressly designed injectors and electronic components to manage the voltage commutation. Moreover, it also revealed a substantial lack of robustness, which may compromise its implementation in a real engine.

Nomenclature

C.I.	: Compression ignition
CNG	: Compressed natural gas
ECU	: Electronic control unit
IGBT	: Insulated gate bipolar transistor
LPG	: Liquefied petroleum gas
MPC	: Model predictive control
OLS	: Ordinary least square
S.I.	: Spark ignition
TTL	: Transistor to transistor logic
E	: Energy transferred to the injector needle during the opening phase
E_{coil}	: Energy stored in the solenoid coil
f_{inj}	: Injection frequency
i	: Solenoid current
L	: Solenoid inductance
m_{exp}	: Experimental injected mass
$\dot{m}$	: Mass flow
R	: Equivalent resistance
t	: Time
t_0	: Time at the end of the rapid discharge phase
V	: Voltage
V_0	: Voltage at the end of the rapid discharge phase
V_1	: Asymptotic voltage of the discharge phase
δ	: Time delay of the injection interruption
ϕ	: Objective function of the optimal condition search algorithm

τ : Duration of the injection interruption
Δt : Injection time
t^* : Opening phase duration

References

[1] M. Cammalleri, E. Pipitone, S. Beccari and G. Genchi, A mathematical model for the prediction of the injected mass diagram of a S.I. engine gas injector, *Journal of Mechanical Science and Technology*, ISSN: 1738-494X, DOI: 10.1007/s12206-013-0848-6 (2013).

[2] J. B. Heywood, Internal combustion engines fundamentals, *McGraw-Hill automotive technology series*, ISBN 0-07-100499-8 (1988).

[3] Bosch *Automotive Handbook*, Robert Bosch GmbH, ISBN 1-56091-918-3 (1996).

[4] Ainul Ghurri, Kim Jae-duk, Song Kyu-Keun, Jung Jae-Youn and Kim Hyung Gon, Qualitative and quantitative analysis of spray characteristics of diesel and biodiesel blend on common-rail injection system, *Journal of Mechanical Science and Technology*, 25 (4) (2011) 885-893.

[5] Hyungmin Kim and Kihyung Lee, An investigation on the fuel behaviour for a PFI type motorcycle engine, *Journal of Mechanical Science and Technology*, 23 (9) (2009) 2507-2513.

[6] Yu Liu, J. K. Yeom and S. S. Chung, An experimental study on the effects of impingement-walls on the spray and combustion characteristics of SIDI CNG, *Journal of Mechanical Science and Technology*, 26 (8) (2012) 2239-2246.

[7] P. Lino, B. Maione and A. Rizzo, Nonlinear modelling and control of a common rail injection system for diesel engines, *Applied Mathematical Modelling*, 31 (9) September (2007) 1770-1784, http://dx.doi.org/10.1016/j.apm.2006.06.001, ISSN: 0307-904X.

[8] X. L. J. Seykens, L. M. T. Somers and R. S. G. Baert, Detailed modelling of common rail fuel injection process, *Journal of Middle European Construction and Design of Cars*, 3 (2-3) (2005) 30, ISSN 1214-0821.

[9] Dat Le, Jin Shen, Neha Ruikar and Gregory M. Shaver, Dynamic modeling of piezoelectric injector-enabled rate shaping, *Proceedings of 2013 American Control Conference (ACC) Washington*, DC, USA, June 17-19 (2013) 3643-3648, ISSN: 0743-1619.

[10] D. Mehlfeldt, H. Weckenmann and G. Stohr, Modeling of piezoelectrically actuated fuel injectors, *Mechatronics*, 18 (5-6) June (2008) 264-272, ISSN: 0957-4158.

[11] M. Baratta, A. E. Catania, E. Spessa, L. Herrmann and K. Roessler, Multi-dimensional modeling of direct natural-gas injection and mixture formation in a stratified-charge SI engine with centrally mounted injector, *SAE International Journal of Engines*, 1 (1) April (2009) 607-626.

[12] S. Di Cairano, A. Bemporad, I. V. Kolmanovsky and D. Hrovat, Model predictive control of magnetically actuated mass spring dampers for automotive applications, *International Journal of Control*, 80 (11) (2007) 1701-1716.

[13] P. Lino, B. Maione, C. Amorese and S. De Matthaeis, Modeling and predictive control of a new injection system for compressed natural gas engines, *Proceedings of the 2006 IEEE International Conference on Control Applications*, Munich, Germany, October 4-6 (2006).

[14] D. Dyntar and L. Guzzella, Optimal control for bouncing suppression of CNG injectors, *Journal of Dynamic Systems, Measurement and Control (ASME)*, 126 March (2004) 47-53.

[15] E. Pipitone and S. Beccari Performances improvement of a S.I. CNG bi-fuel engine by means of double-fuel injection, *SAE technical paper 2009-24-0058*, DOI: 10.4271/2009-24-0058.

[16] E. Pipitone and S. Beccari, Performances and emissions improvement of an S.I. engine fuelled by LPG/gasoline mixtures, *SAE technical paper 2010-01-0615*, DOI: 10.4271/2010-01-0615.

[17] G. Genchi, E. Pipitone, S. Beccari and A. Piacentino, Knock resistance increase through the addition of natural gas or LPG to gasoline: An experimental study, *SAE Technical Paper 2013-24-0100*, DOI:10.4271/2013-24-0100.

[18] Fairchild Semiconductor Corporation, *HGTP14N40F3VL/HGT1S14N40F3VLS Data sheet Rev. B1*, February (2002).

Appendix

A.1 Extra current sub-model

The first tests on interrupting the injection pulse, which aimed to modulate the energy transferred to the needle, showed a phenomenon not observed in the previous work. The experimental data effectively revealed an extra current, whose duration and magnitude depend on the duration of the pulse interruption, as shown in Fig. A.1. Here, different solenoid current waveforms, obtained by varying the pulse interruption duration, are represented as a function of time. The amplitude of the extra current decreases when the interruption duration increases.

The analysis of the injection electric circuit (see Fig. A.2) and the characteristics of the insulated gate bipolar transistor (IGBT) [18], together with some voltage measurements (carried out between points A and B of the electric circuit) led the authors to believe that the phenomenon is related to the dissipative discharge of the energy stored in the solenoid coil.

When the injection is interrupted, the IGBT is deactivated, which in turn suddenly opens the electric circuit (between points A and B). The solenoid current immediately falls to zero, which causes an abrupt decrease in the solenoid magnetic flux, which according to the Faraday-Lenz law induces a very high voltage in the solenoid. A waveform of this high voltage was recorded by means of a 100 MHz oscilloscope and is reported in Fig. A.3. The voltage induced in the solenoid circuit fully exceeds 390 V (which is also the maximum visible value of the oscilloscope). As a consequence, the IGBT intrinsic protection system, endowed with Zener diodes and internal resistance, allows this high voltage to discharge itself toward the ECU ground (current i_1 in Fig. A.2). The first part of the solenoid energy discharge is very rapid, as shown in Fig. A.3.

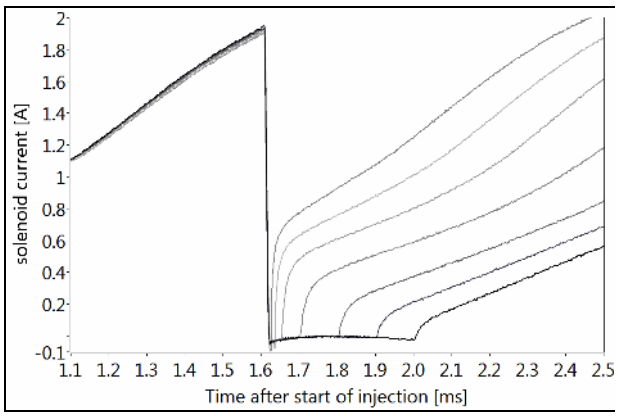

Fig. A.1. Measured solenoid current of various durations of pulse interruption.

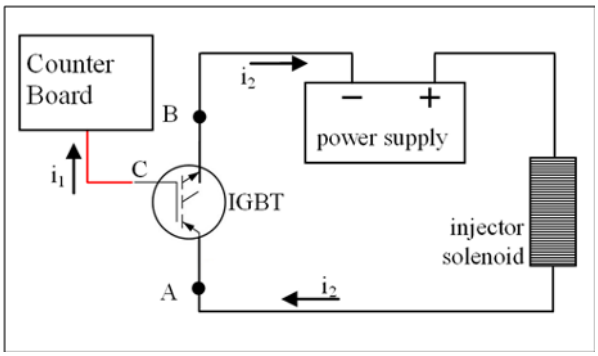

Fig. A.2. Electrical circuit involved in the injector operation.

Once a voltage of about 130 V is reached (i.e., approximately 0.02 ms after the start of the pulse interruption) as a result of the IGBT intrinsic protection system properties [18], the path to the ECU ground through the IGBT closes. Consequently, the energy continues to discharge through the internal structure of the injector itself. This second stage of the discharge process is slow, and the voltage exhibits a gradual decrease, as Fig. A.3 shows.

Considering a simple R-L circuit, this voltage waveform is fitted by an exponential function of time t:

$$V = V_1 + (V_0 - V_1) \cdot e^{-(t-t_0)\frac{R}{L}} \tag{A.1}$$

where t_0 and V_0 represent the time and voltage at the end of the rapid discharge phase (0.02 ms and 130 V, respectively), V_1 is the asymptotic voltage (given by the power supply system), and L/R is the time constant of the circuit. In particular, L is the known solenoid inductance, and R is the equivalent resistance of both the solenoid and the power supply system, which is determined by fitting the data in Fig. A.3 with Eq. (A.1).

The instantaneous energy stored in the solenoid can always be expressed as follows:

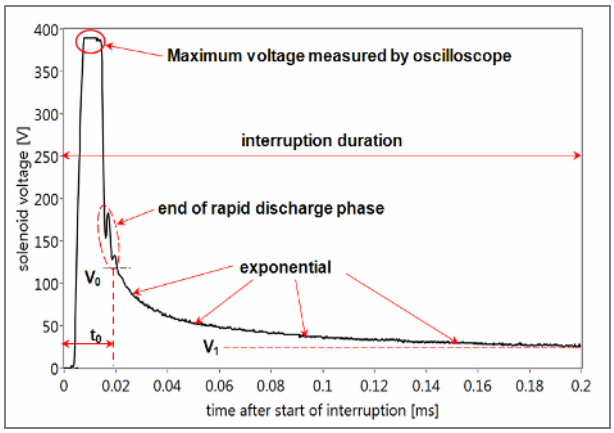

Fig. A.3. Measured solenoid voltage during the injection pulse interruption.

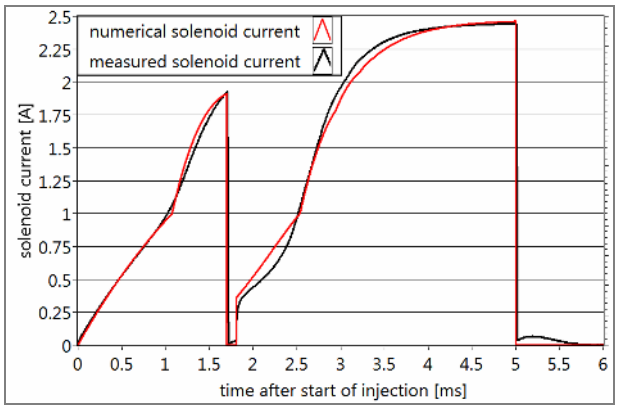

Fig. A.4. Injection pulse interruption: measured and simulated solenoid current for air at 10 bar.

$$E_{coil} = \frac{1}{2} \cdot L \cdot i(t)^2 \tag{A.2}$$

where according to Eq. (3), the current *i(t)* during the slow discharge phase can be evaluated as:

$$i = \frac{(V_0 - V_1)}{R} \cdot e^{-(t-t_0)\cdot\frac{R}{L}}. \tag{A.3}$$

If, during this slow discharge phase, the electric circuit is closed again (i.e., the IGBT is reactivated) after a sufficiently short time (less than 0.2 ms from the start of the pulse interruption), then the residual energy still stored in the solenoid is suddenly discharged through the power supply cathode. This sudden discharge produces the extra current (i_2 in Fig. A.2), whose value depends on the energy still available in the solenoid, and can therefore be evaluated by Eq. (A.3). It is also obviously related to the duration of the interruption, thereby explaining the current waveforms represented in Fig. A.1.

Eqs. (A.1) and (A.3) are used in the model to take account for the phenomenon of the extra current. Fig. A.4 shows a good agreement between the experimental measure and simulation output.

Stefano Beccari obtained his Ph.D. in Mechanical Engineering from University of Palermo (Italy) in 2005. He is currently a Researcher at the University of Palermo in the field of fluid machines. His main research interests include spark ignition engine performance and efficiency optimization, with particular reference to the bi-fuel engines: gasoline-natural gas and gasoline-LPG.

Emiliano Pipitone graduated in 1999 with a degree in Mechanical Engineering from the University of Palermo, where he has been an Assistant Professor in the field of fluid machinery, energy systems, and power generation since March 2001. He is currently a lecturer in "Fluid Machinery" and "Internal Combustion Engine" and is the head of the Internal Combustion Engine Laboratories of the Department. He conducted experimental and theoretical studies on internal combustion engine fuel injectors, combustion diagnosis and optimal phase control, detection and measurement of knocking phenomena, fluid dynamics of engine intake systems, as well as engine modeling and use of gaseous fuels for spark ignition engines.

Marco Cammalleri graduated in 1998 with a degree in Mechanical Engineering from the University of Palermo, where he has been an Assistant Professor since July 2000 and a teacher of the mechanics of the machines since 2001. His current studies focus on the dynamics of an SI engine fuel gas injector, rotor dynamics and mechanical vibrations, and mechanism design. He has previously conducted theoretical and experimental research on single and split way CVT transmissions and on rubber v-belt mechanics.

Giuseppe Genchi graduated in 2009 with a degree in Mechanical Engineering from the University of Palermo (Italy). He obtained his Ph.D. in Energetics from the University of Palermo (Italy) in 2014. He is currently a Researcher at the University of Palermo in the field of fluid machines. His main research activities focus on the simultaneous combustion of gaseous fuel and gasoline mixtures in SI engines, particularly on the octane rating and supercharged engine application of the natural gas-gasoline and LPG-gasoline mixtures.